Evolution of the electronic structure in Mo$_{1-x}$Re$_x$ alloys

Michio Okada[1,2,10]**, Eli Rotenberg**[3]**, S D Kevan**[3,4]**, J Schäfer**[5]**, Balazs Ujfalussy**[6,7]**, G Malcolm Stocks**[7]**, B Genatempo**[8]**, E Bruno**[8] **and E W Plummer**[9]

[1] Department of Chemistry, Graduate School of Science, Osaka University, 1-1 Machikaneyama-cho, Toyonaka, Osaka 560-0043, Japan
[2] 8-1 Mihogaoka, Ibaraki, Osaka 567-0047, Japan
[3] Advanced Light Source, Lawrence Berkeley National Laboratory, Berkeley, CA 94720, USA
[4] Department of Physics, University of Oregon, Eugene, OR 94703, USA
[5] Physikalisches Institut, Universität Würzburg, Am Hubland, D-97074 Würzburg, Germany
[6] Wigner Research Centre for Physics, Hungarian Academy of Sciences, Budapest, Hungary
[7] Metals and Ceramics Division, Oak Ridge National Laboratory, Oak Ridge, TN 37831-6057, USA
[8] Departmento di Fisica, Univerita di Messina, Salita Sperone 31, I-98166 Messina, Italy
[9] Department of Physics and Astronomy, Louisiana State University, Baton Rouge, LA 70803-4001, USA
E-mail: okada@chem.sci.osaka-u.ac.jp

Abstract. We report a detailed experimental and theoretical study of the electronic structure of Mo$_{1-x}$Re$_x$ random alloys. We have measured electronic band dispersions for clean and hydrogen-covered Mo$_{1-x}$Re$_x$(110) with $x = 0$–0.25 using angle-resolved photoemission spectroscopy. Our results suggest

[10] Author to whom any correspondence should be addressed.

that the bulk and most surface electronic bands shift relative to the Fermi level systematically and approximately rigidly with Re concentration. We distinguish and quantify two contributions to these shifts: a raise of the Fermi energy and an increase of the overall bandwidth. Alloy bands calculated using the first-principles Korringa–Kohn–Rostoker coherent-potential-approximation method accurately predict both of these effects. As derived from the rigid band model, the Fermi energy shift is inversely related to the bulk density of states in this energy region. Using our results, we also characterize an electronic topological transition of the bulk Fermi surface and relate this to bulk transport properties. Finally, we distinguish effects beyond the rigid band approximation: a highly surface-localized state and a composition-dependent impact of the spin–orbit interaction.

Contents

1. Introduction

Metal alloys remain a cornerstone of many technologies, both modern and ancient. However, despite many decades of effort to understand their properties from first principles, relatively little predictive power exists to allow development of alloys with properties tuned for specific applications [1]. Part of the reason for this is the paucity of detailed investigations of alloy electronic structure. For example, some alloy properties depend on variations in Fermi surface topology that can be induced by alloying. Mott's early rigid band model (RBM), in which the band structure and density of states (DOS) of the solvent metal remain unchanged upon alloying with a solute metal allows these variations to be predicted [2]. However, the validity of the RBM has been shown to be rather limited both by experiment [3, 4] and by theory [5–8]. Whereas rigid band behavior has been confirmed for many nearly free electron and some transition metal systems [9–11], its applicability has remained questionable where the solute strongly perturbs the local electronic structure of the solvent. Even in systems such as $Mo_{1-x}Re_x$, where the RBM has been assumed to be applicable [11–14], few experimental studies have been reported that provide microscopic information about how the electronic structure evolves with alloying.

To be fair, modern computer simulations coupled with experimental binary phase diagrams show promise in the design of high strength, high conductivity alloys for applications under extreme conditions [1].

The recent discovery of high-temperature superconductivity in the layered iron-based compounds [15] has also created a new challenge for modern alloy theory, because in many cases alloying is what induces superconductivity. The isovalent alloy $FeTe_{1-x}Se_x$ exhibits superconductivity over a wide doping range for $x > 0.45$ [16–18]. In this doping range the alloy is not random, but the electronic properties are homogeneous. The dilute alloy $Ba(Fe_{1-x}Co_x)_2As_2$ exhibits superconductivity for $\sim 0.03 < x < \sim 0.15$ [19], where the presence of Co decreases the magnetic and structural transitions temperatures and induces superconductivity. Understanding the physical properties of such complex alloys containing transition metals would be facilitated by a detailed picture of the evolution of the conduction states in simpler binary transition metal alloys, such as $Mo_{1-x}Re_x$ alloys.

The changes in alloy band structure and Fermi surface can now be modeled using modern electronic structure calculations based on the coherent potential approximation (CPA) [20–22], but corresponding experimental studies of alloy band structure using angle-resolved photoemission are rare. Part of the reason for this is the surface sensitivity of photoemission coupled to stoichiometry variations typically observed near the surface of an alloy. In this paper, we report a detailed experimental and theoretical study of $Mo_{1-x}Re_x$ random alloys where the near-surface stoichiometry is known to be very close to that of the bulk [23]. We do this both by calculating the evolution of alloy band structure as a function of composition using the Korringa–Kohn–Rostoker (KKR)-CPA method and also by directly measuring this evolution using angle-resolved photoemission spectroscopy (ARPES). Re ($5d^5 6s^2$) has one more electron per atom than Mo ($4d^5 5s^1$), which in the RBM would be shared with the molybdenum host. As predicted by the RBM, we find that the bulk and also surface electronic bands shift away from the Fermi energy (E_F) with increasing Re concentration. However, this shift is not uniform throughout the occupied portion of the band structure, with larger shifts being observed at higher binding energy. We distinguish and quantify two components to these shifts: (i) rising of the Fermi energy due to the aforementioned charge donation and (ii) increasing of the occupied bandwidth, most notably for bands more than 2 eV below E_F. Given the observed behavior near E_F, we are also able to measure a predicted electronic topological transition (ETT) [11, 24]. An ETT occurs when the Fermi surface changes its topology as E_F moves through a van Hove singularity in the DOS. Such ETTs can be accompanied by drastic changes in the DOS at the Fermi level, $N(E_F)$, and thereby may impact many physical properties of alloys [11, 24–28]. We will demonstrate experimentally how the observed band shift induces an ETT close to the predicted concentration. Finally, we distinguish two other deviations from rigid band behavior. First, we find that a highly surface-localized state shifts in a notably non-rigid fashion. Also, the impact of the spin–orbit interaction increases with increasing rhenium concentration, leading to non-rigid shifts of some bands.

2. Experimental and computational approaches

ARPES experiments were performed at beamline 7.0 of the Advanced Light Source at photon energy of 100 eV. The base pressure of the ARPES chamber was 8×10^{-11} Torr. The combined monochromator and energy analyzer energy resolution was ~ 80 meV, and the momentum resolution was a few per cent of the width of the Brillouin zone. $Mo_{1-x}Re_x(110)$ ingots with

IOP Institute of Physics ⏀ DEUTSCHE PHYSIKALISCHE GESELLSCHAFT

$x = 0.00$, 0.05, 0.15 and 0.25 were grown by the crystal-growth group in the Solid State Division at Oak Ridge National Laboratory. Slices of $Mo_{1-x}Re_x(110)$ were cut from the ingots and polished within $0.3°$ of the (110) orientation, as determined by Laue back-reflection. The samples were mounted individually on a high-precision ultrahigh vacuum goniometer and could be cooled with liquid nitrogen to $< 130\,K$ and also heated by electron bombardment to about $2100\,K$. The $Mo_{1-x}Re_x(110)$ samples were cleaned by several cycles of oxidation at $1500\,K$ followed by sublimation of the oxide at $2000\,K$. For $x \leqslant 0.35$, $Mo_{1-x}Re_x$ is a random alloy where Mo and Re atoms are randomly distributed on a bcc lattice, and the composition of the top layer for (110) surfaces has been shown to be essentially the same as in the bulk [23]. Surface and bulk electron states were distinguished by their sensitivity to contamination.

The electronic structure of $Mo_{1-x}Re_x$ alloys was calculated using the first-principles KKR-CPA method [29–33]. The KKR-CPA is a first-principles theory of the electronic structure of random solid solution alloys [29, 30] in which electronic structure problem is solved using multiple scattering theory Green's function methods and the effects of disorder on the electronic structure are treated using the CPA. The CPA can be viewed as a mean field theory that provides the best single-site theory of the effects of disorder on the electronic structure. The KKR-CPA allows *direct* calculation of the configurationally averaged properties of the alloy—configurationally averaged DOS, charge density and Bloch spectral function (BSF) [31]. In the limit of a pure metal or ordered compound, the KKR-CPA reduces to the KKR band structure method. Implemented within the local density approximation (LDA) and using density functional theory (DFT), the LDA-KKR-CPA method is a totally parameter-free theory [32, 33]. In particular, the LDA-KKR-CPA satisfies many of the variational properties of conventional LDA-DFT, save that it is generalized to configuration-averaged single-site quantities. The results presented in this work are based on a fully relativistic implementation of the KKR-CPA (Rel-KKR-CPA) method based on solution of the Dirac equation. $Mo_{1-x}Re_x$ alloys have been studied previously using these methods, particularly within the context of ETTs [17]. Specifically, the results presented here are based on the same code as those of Bruno and Ginatempo [34] and as such are consistent with that work. The densities of states (DOS) and BSF for the endpoint pure metals Mo and Re both in the bcc structure (recall that pure Re is actually hcp) are shown in figure 1. As can be seen in both the DOS and BSF, the major differences between Mo and Re are a rise in the Fermi energy of Re relative to Mo due to the addition of an extra electron and a significant broadening of the occupied band. This latter effect is primarily due to relativistic effects, which are much larger in Re (atomic number 75) than in Mo (atomic number 42). The mass–velocity and Darwin terms result in a downward shift in the sp-states relative to the d-states—note the much larger separation between the lowest two Γ-states in Re than in Mo. Spin–orbit coupling terms then resolve certain degeneracies present in the non-relativistic and semi-relativistic theories. Again these effects are negligible in the Mo and are significant in Re: note that the energies of second (doublet) and third (singlet) lowest Γ-point states is much larger in Re ($\sim 0.63\,eV$) than in Mo ($\sim 0.15\,eV$).

3. Computational results

3.1. Alloy density of states

The calculated DOS for $Mo_{1-x}Re_x$ alloys having an atomic fraction of Re $x = 0.00$, 0.05, 0.15 and 0.25 are shown in figure 2. The calculations are for an underlying ideal bcc structure and
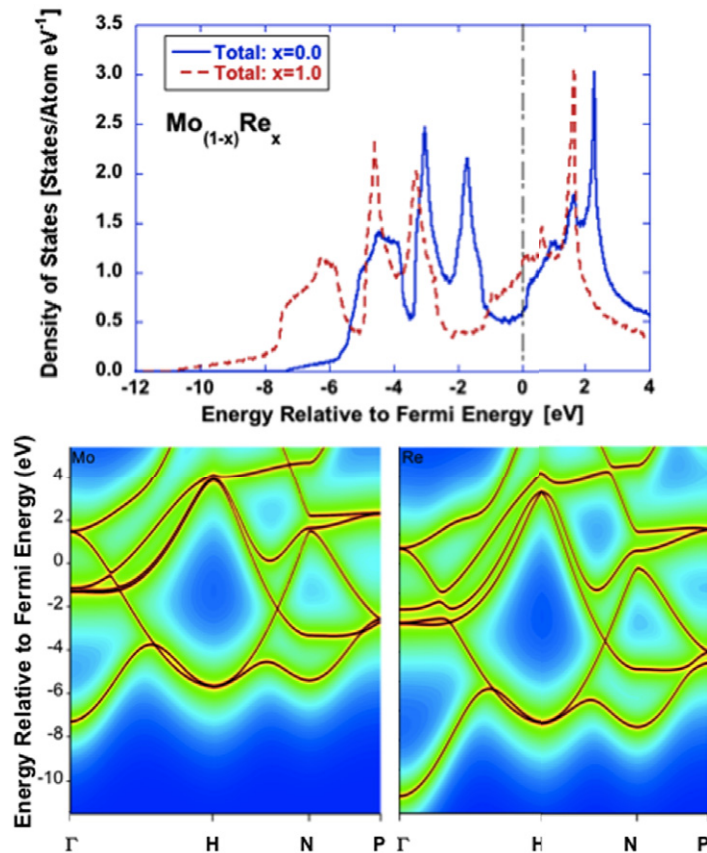
Figure 1. DOS (above) and band structures of bcc Mo and Re calculated using the Rel-KKR-CPA method. The lattice parameters, a_0, of Mo and Re were taken to be 5.947 and 5.834 Bohr. The Re lattice parameter corresponds to a bcc lattice having the experimentally determined atomic volume of hcp phase.

a lattice spacing corresponding to a Vegard's rule interpolation of those appropriate to Mo ($a_0 = 5.947$ Bohr) and Re ($a_0 = 5.834$ Bohr). The latter is an equivalent bcc lattice spacing corresponding to the experimental atomic volume of hcp Re. Of particular note is the relative sharpness of the DOS across the complete concentration range. The major changes in the DOS accompanying the addition of Re are (i) an overall shifting down of the DOS due to the addition of the extra electron of Re, (ii) a gradual widening (stretching) of the both the narrow, high DOS, tight-binding like d-band and broad, low DOS, free electron like sp-band and (iii) a gradual rounding of the sharp structures in the DOS. As for the Mo and Re-component, the three major peaks below Fermi energy (E_F) are present in both, albeit the maximum of each peak is very slightly lower in energy for the Re-component than for the Mo-component. Of these three, only the former is consistent with common or rigid-band behavior. Thus the presence of the band stretching and increased spin–orbit splitting in Re relative to Mo can be expected to make the concentration dependence of individual states depend on their position relative to E_F and as well as their spin and orbital character.
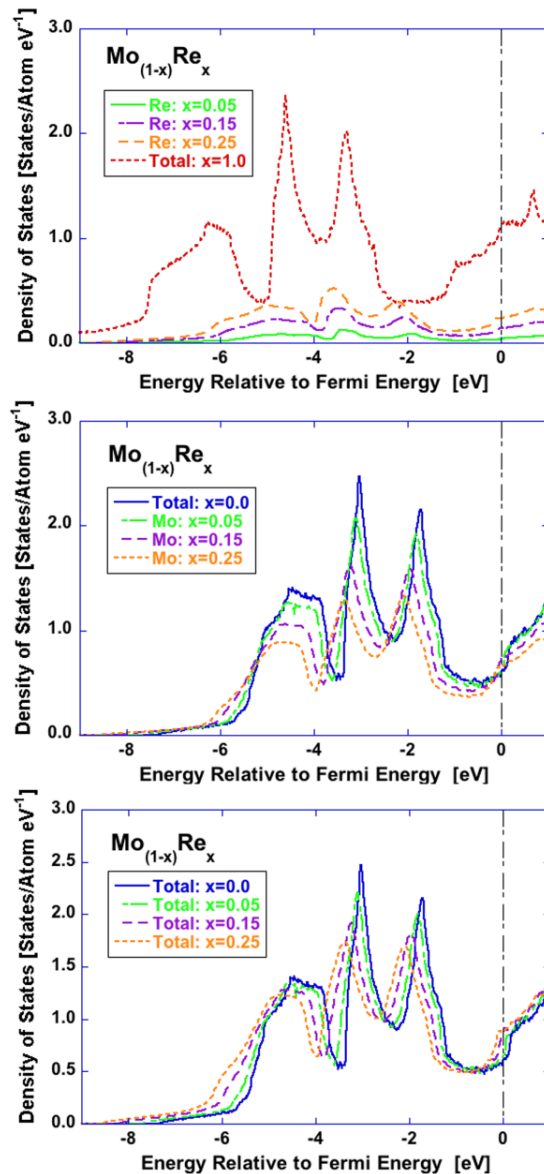
Figure 2. Configurationally averaged DOS of $Mo_{1-x}Re_x$ ($x = 0.00, 0.05, 0.15, 0.25$ and 1.0) calculated using the Rel-KKR-CPA method. Lower: total DOS; middle: contribution from Mo-sites; and upper: contribution from Re-sites.

3.2. Bloch spectral function and alloy band structure

The most important quantity for interpretation of angle-resolved photoemission experiments is the BSF, $A_B(\boldsymbol{k}, \varepsilon)$, which is the generalization to substitutionally disordered alloys of the band structure of the end point pure metals [27]. For ordered (periodic) systems, the BSF is a set of delta functions at the band energies, for weak disorder the delta functions are broadened into Lorentzian peaks with a well-defined width. For stronger disorder, peaks in the BSF can no longer be clearly identified with specific states in any corresponding ordered system. For weak
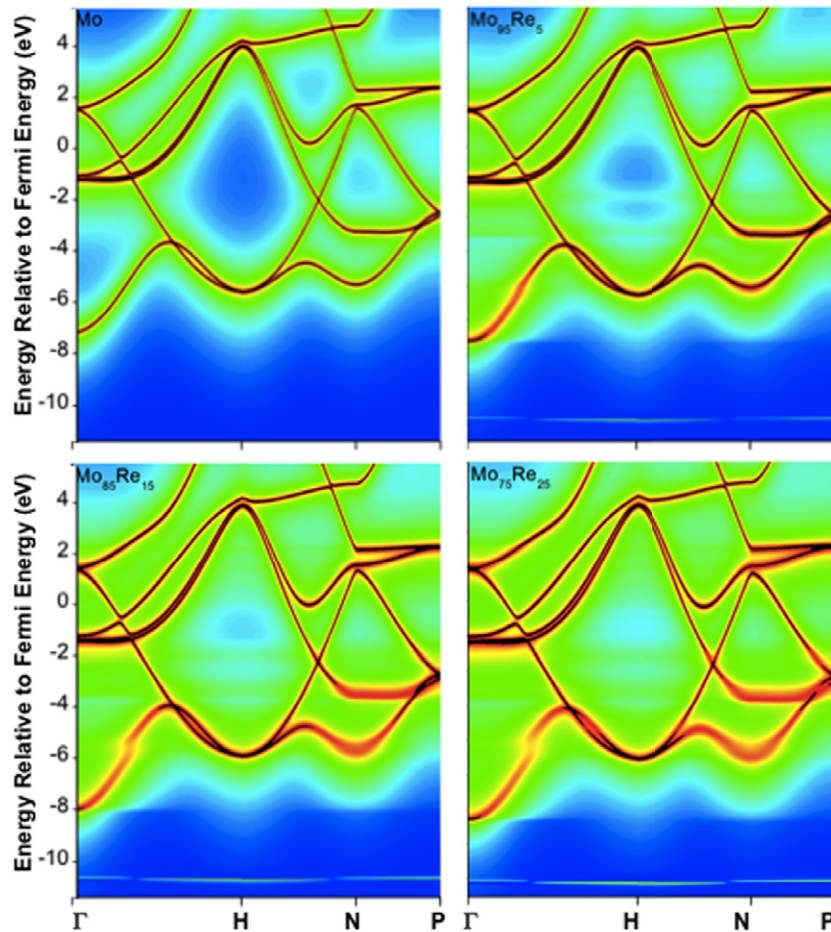
Figure 3. Bloch Spectral Function (BSF) along high symmetry directions in the Brillouin zone for bcc $Mo_{1-x}Re_x$ alloys atomic fractions $x = 0.00$, 0.05, 0.15 and 0.25 (left to right and top to bottom) calculated using the Rel-KKR-CPA method, the lattice parameters used in the calculations were the same as those of figure 2.

disorder, the inverse of the k-width is directly related to the mean free path; alternatively, the inverse of the width in energy measures the k-dependent lifetime of the states.

In figure 3, we have plotted the BSF as a function of energy and k-vector along several high symmetry directions in the bcc Brillouin zone (Γ–H–N–P). When reading these figures, it should be noted that the BSF is actually calculated on an energy contour that is parallel to the real axis but displaced by 1 mRyd into the complex plane. Although this device results in an additional broadening, over and above that due to the alloy disorder, it is small as can be seen by comparing the BSF of the pure metals in figure 1, where the broadening results entirely from the small imaginary part in the energy, with those of the alloys of figure 3 where the broadening results primarily from the compositional disorder. This notwithstanding, the overall sharpness of the BSF is apparent; for none of the alloy 'bands' is the disorder broadening (full-width at half-maximum) greater than $\sim$100 meV. Given the sharpness of the peaks in the BSF, it is possible to define an alloy band structure through effective 'ε versus k' relation as the locus of
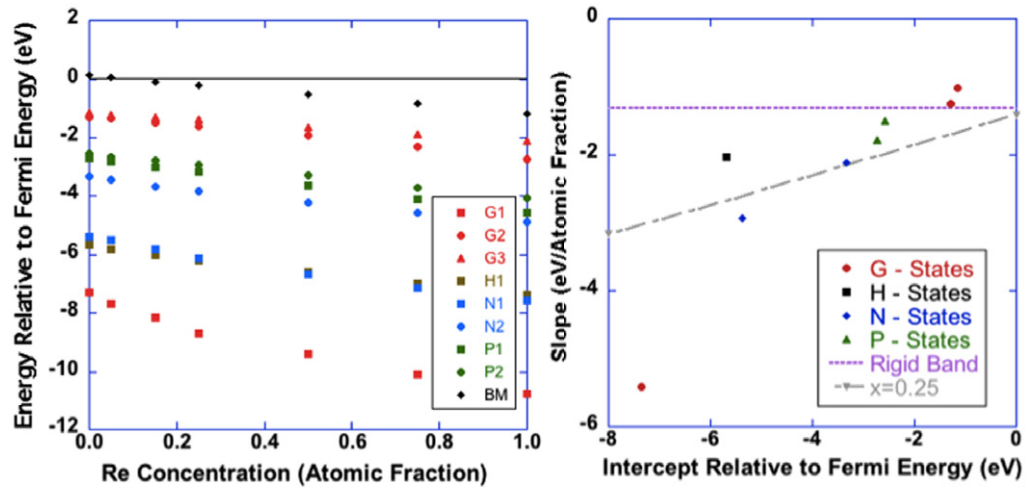
Figure 4. (Left) Calculated dependence of BSF peak positions on Re-content at a number of k-points (Γ, H, N, P and the band minimum (BM) along the H–N direction referred to in the text) in the bcc Brillouin zone based on the Rel-KKR-CPA data of figure 3. Multiple states at a single k-point are labeled numerically in order of increasing energy. (Right) A plot of the slope (y-axis) and intercept (x-axis), at zero concentration (i.e. pure Mo), of a linear least square fit to the concentration dependence of the energy of each of the states depicted in the left frame. Only the experimentally relevant compositions ($x \leqslant 0.25$) were used in the fitting procedure to the data of the left figure. The dashed (purple) line corresponds to the rigid band slope based on the DOS of pure Mo. The dot-dashed (gray) line corresponds to the experimental slope for $x = 0.25$; $\alpha^k = -1.41 + 0.22 E_B$ (also see text).

the well-defined peaks in the BSF. This then allows us to track the concentration dependence of individual states in this generalized band structure.

In figure 4, we show the concentration dependence of the positions of various occupied states for the relativistic BSFs shown in figures 2 and 3 as well as for two other concentrations, $x = 0.5$ and 0.75 (not shown). At each symmetry point, we have labeled the peaks in the BSF according to the symmetry point (Γ, H, N, P) and an index enumerating the states in increasing energy. The curve labeled band minimum (BM) is for the k-point along the H–N direction corresponding to the BM that is evident in the BSFs shown in figure 3. The behavior of this band will be of consequence for later discussion of an ETT.

Given that the states at the high symmetry points are so well defined, it is tempting to label the peaks according to the symmetry of the corresponding band states of the pure elements despite the fact that the peaks in the BSF do not correspond to Block states of a single, well-defined, k-vector and as a consequence no such labeling is warranted. Despite this, it is also true that the peak labeled G1 corresponds to the Bloch state conventionally labeled Γ_6^+ and the peaks labeled G2 and G3 correspond to the Γ_8^+ and Γ_7^+ states, respectively. From this notation, it is also clear that the energy difference between the peaks labeled G2 and G3 is a measure size of the spin–orbit splitting between the Γ_7^+ and Γ_8^+ states of the pure metals; we return to this point in section 4.3.
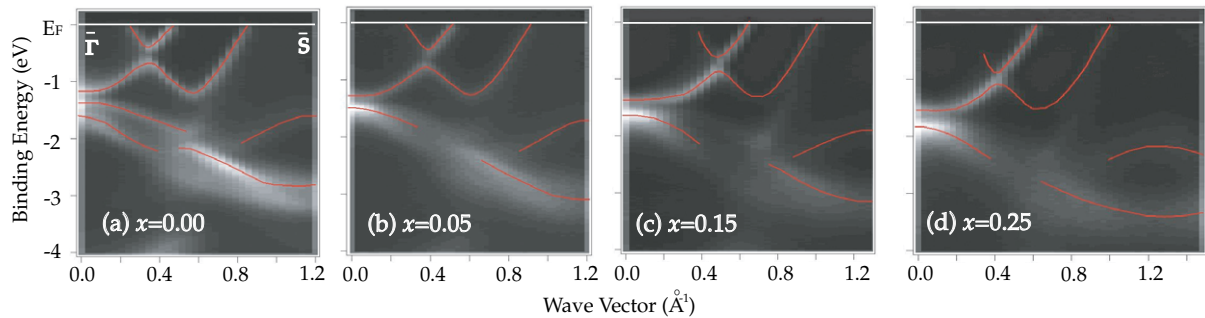
Figure 5. Valence band maps of $Mo_{1-x}Re_x(110)$ for (a) $x = 0.00$, (b) 0.05, (c) 0.15 and (d) 0.25, along the $\overline{\Gamma}–\overline{S}$ direction on the SBZ. Superposed curves indicate the underlying dispersion relations are guides to the eye.

As is clear from figure 4 (left), at low Re concentration (the $x \leqslant 0.25$ concentration range relevant to our experiments) the dependence of the peak positions is essentially linear in alloy composition excepting for the lowest level (G1) where there is some nonlinear compositional dependence for high Re content. Beyond this linear concentration dependence of all of the band shifts at $x \leqslant 0.25$, the slope of the band shifts generally increases the further below the Fermi energy the particular band is. This is quantified in figure 4 (right) where we show the relationship of the coefficient ε_0^k and α^k of a linear least-squares fit of the form $\varepsilon_{\text{alloy}}^k(x) = \varepsilon_0^k + \alpha^k x$ to the concentration (x) variation of the alloy band energy ($\varepsilon_{\text{alloy}}^k(x)$) of the k-points studied. While there is no simple linear relationship between the slope (α^k) and intercept (ε_0^k), in general the more negative the intercept the larger the slope, which is then a measure of the 'band stretching' effect that accompanies the addition of Re to Mo. The effect is small for states near the Fermi energy ($\varepsilon \leqslant 2\,\text{eV}$) but is very large for the lowest lying, Γ-centered, s-state at the bottom of the occupied band.

4. Experimental results

4.1. Rigid band behavior of a single band

Figure 5 presents ARPES band maps that illustrate the Re concentration dependence of the alloy electronic structure along the $\overline{\Gamma} \to \overline{S}$ line in the surface Brillouin zone (SBZ) illustrated in figure 6. As indicated by the curves superposed on the gray-scale band maps, the underlying energy bands shift systematically and approximately rigidly away from E_F with increasing Re concentration. Figure 7(a) summarizes the experimental dispersion relations extracted from these band maps. To account for small misalignment of our crystals ($< 0.5°$), these dispersion relations were shifted by small amounts along the horizontal axis to ensure alignment of band extrema. An approximately rigid shift is now readily apparent for bulk and surface bands alike. The band labeled A, for example, is a surface state as it crosses E_F, but merges with the bulk continuum near zone center and is essentially the bulk $\Gamma_{25'}$ band at zone center. Deeper bands are generally bulk states. Similar band map measurements were performed along the $\overline{P}–\overline{S}–\overline{H}$ and the $\overline{S}–\overline{\Sigma}–\overline{S}$ directions, with similar results.

As noted in the previous section, the downward shift of the d-derived surface and bulk bands can be understood qualitatively within the context of the RBM since rhenium has one
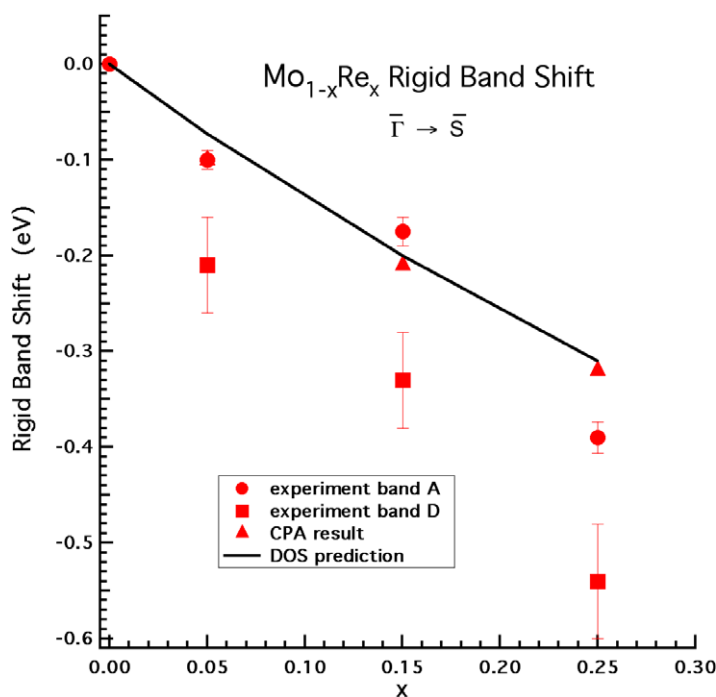
Figure 6. Bulk and related (110) SBZ for the bcc lattice.

Figure 7. (a) Measured dispersion relations for $Mo_{1-x}Re_x(110)$ along the $\overline{\Gamma} \to \overline{S}$ line of the SBZ, extracted from the band maps in figure 5. Data have been shifted horizontally by small amounts to account for sample misalignments. (b) Dispersion relations from panel (a), with the alloy results shifted so as to align band A as well as possible. (c) Dispersion relations from panel (a) with the alloy results shifted and stretched as described in the text to demonstrate and quantify the rigidity of the alloy-induced band shift. The shaded region is the projection of the pure molybdenum bulk bands onto the (110) SBZ.

more valence electron than molybdenum. To test the RBM for a single band, in figure 7(b) we have shifted the alloy bands vertically to overlay the dispersion relations of band A as well as possible. This procedure clearly collapses the results for band A from all the alloy surfaces onto

Figure 8. Experimental and calculated rigid band shifts for $Mo_{1-x}Re_x(110)$. Filled circles: shifts for band A deduced from the analysis in figure 7(b). Filled squares: measured shifts for band D in figure 7. Solid curve: rigid-band shift predicted based on filling the bulk molybdenum DOS. Filled triangles: typical band shifts calculated using the CPA.

a single curve, verifying the approximately rigid shift. Moreover, the results for band B also located near E_F and for band C near the zone boundary collapse using the shifts derived from band A.

This is an important observation, since bands A and B are associated with different segments of the Fermi surface. They could, in principle, shift rigidly, although at different rates, while still allowing the system to maintain overall charge neutrality. That is not the case, and the RBM appears to be followed in a strict sense. The shifts deduced in this way are plotted as filled circles in figure 8 with error bars that reflect the standard deviation between the shifted alloy and the pure molybdenum band. The shift is measured to be rigid with a precision better than 40 meV, compared to a total shift an order of magnitude larger.

The observed shift of bands A–C compare favorably to the predictions of the RBM as well as to shifts calculated from first principles in section 3. In the RBM, the rate of shift of the bulk band is predicted to be inversely related to the bulk DOS at and above E_F. The bulk molybdenum DOS near E_F, calculated using the KKR-CPA approach explained above, is similar to that predicted from the interpolation scheme of Papaconstantopoulos [35] and also to that reported in the literature [11, 24]. We integrated this DOS above E_F to predict the RBM shift rate shown in figure 8. The match between experiment and theory is seen to be quite good. Alternatively, as explained in section 3, the first-principles KKR-CPA calculation also quantified a very nearly rigid shift of several alloy bands near E_F. These first-principles calculated shifts

Table 1. Rigid band parameters.

x	$\alpha(x)$ (eV)	$\beta(x)$
0.05	-1.17 ± 0.23	0.93 ± 0.16
0.15	-1.03 ± 0.16	0.26 ± 0.11
0.25	-1.41 ± 0.11	0.22 ± 0.08

closely match those based on the molybdenum DOS, and also our experimental result. We will quantify this comparison below.

Despite this successful application of the RBM to a single band near E_F, a simple Fermi-level shift cannot explain all of our results in detail. It is apparent in figure 7(b) that the shifts with alloy composition of the deeper bulk bands, while approximately rigid, are of systematically larger magnitude than for the bands closer to E_F. For example, we plot the measured shift of band D in figure 8, and find that the rate of shift is nearly a factor to two larger than for band A. This stretching of the bands at binding energies greater than about 2 eV was predicted by the KKR-CPA calculation described in section 3.

For more detailed analysis of experimental data, we attempt to quantify these shifts using an empirical relationship of the form

$$\Delta E = (\alpha + \beta E_B)x, \tag{1}$$

where x is the rhenium atomic fraction, α is a parameter that accounts for the shift of the Fermi level and β accounts for a stretching of the bands that, we assume, depends linearly on the binding energy E_B. For a collection of many points along three different lines in the Brillouin zone, we plot the measured alloy shift divided by the rhenium concentration (not shown here), against the binding energy of the band for the pure molybdenum surface. The points for each alloy composition are reasonably well described by a single straight line. This is as predicted in equation (1), except that α and β are found to depend on x. The derived values of $\alpha(x)$ and $\beta(x)$ are given in table 1. Our results suggesting $\beta \neq 0$ reflect a breakdown of the RBM in the sense that the occupied bandwidth below E_F increases faster than the RBM would predict. Bands near the Fermi level will shift at a rate inversely related to the bulk DOS to maintain charge neutrality. Deeper bands will experience that band filling shift augmented by a shift associated the increasing alloy bandwidth. We applied this empirical 'shift and stretch' algorithm from equation (1), using the data in table 1, to transform the alloy bands in figure 7(a). The result, plotted in figure 7(c), shows that the bands for all four alloys can be brought into very good alignment with this empirical procedure, with the exception of the lower-lying band at zone center. This band is actually a doublet on the pure molybdenum surface that is not resolved on the alloy surfaces, so we do not trust our analysis of these data. While the band shifts are not uniform below E_F, figure 7(c) demonstrates that the band shapes are preserved to roughly ± 50 meV, compared to a total shift about an order of magnitude larger, and individual bandwidths of 1–2 eV. For $x = 0.25$, we plot the slope ($\alpha^{\mathbf{k}} = a + bE_B$ determined from $\alpha(x)$ and $\beta(x)$ given in table 1 in figure 4. The KKR-CPA calculation reproduces the band shift and stretching reasonably.

4.2. Electronic topological transition

We now turn our attention to the existence of an ETT in this system. A recent first-principles calculation of the bulk electronic structure of $Mo_{1-x}Re_x$ alloys by Skorodumova *et al* [11] predicts that two ETTs will occur near the middle of the N–H line in the bulk Brillouin zone at 2 and 6% Re concentration. This region projects (see figure 6) onto the SBZ near the boundary between $\overline{S}$ and $\overline{P}$. In our experimental results, the finite mean free path of the photoelectron means that we sample 20–25% of the bulk BZ in the direction perpendicular to the surface. In the vicinity of the ETT, it is therefore appropriate to compare the photoemission data to projections of the bulk band structure onto the SBZ. The band maps along the $\overline{P} \to \overline{H}$ for $x = 0.00$ and 0.25, shown in figures 9(a) and (b), respectively clearly indicate this ETT. An 'extra' peak marked by the arrow in figure 9(b) appears very clearly on the alloy surface close to E_F between $\overline{P}$ and $\overline{S}$. This peak is produced as the Fermi level sweeps through a BM upon alloying, i.e. it reflects an ETT. Band maps on the other alloy surfaces indicate that the band just becomes visible at 5% rhenium concentration, or very close to the high concentration ETT predicted by Skorodumova *et al* [11].

The experimentally determined projected Fermi surface confirms this interpretation. Figures 9(c) and (d) present a map of the photoemission intensity near the Fermi level for pure Mo and $Mo_{0.75}Re_{0.25}$. The band that falls below E_F in figure 9(b) fills the gap around the yellow point labeled F with increasing Re concentration. In pure molybdenum, segments of the bulk Fermi surface in the first and second Brillouin zones are not connected, as indicated by the blue dashed lines. Upon alloying, these two orbits grow and eventually connect to form a channel, as indicated by the dashed lines in figure 9(d). Similar data at other concentrations indicate that contact occurs at or slightly above 5% Re concentration. To compare these photoemission data with calculation, we have projected constant energy contours of the bulk Mo band structure [35] onto the (110) SBZ at E_F and $E_F + 0.4$ eV, corresponding to the shift of band A on $Mo_{0.75}Re_{0.25}$. The results, shown in figures 9(e) and (f), predict the gross topological changes associated with the ETTs near the $\overline{S} \to \overline{P}$ SBZ boundary and confirm our interpretation. By projecting at intermediate energy shifts, we find that a tube bridges the projected band gap between $\overline{P}$ and $\overline{S}$, making contact at a rhenium concentration just above 5%, as observed.

The ETT confirmed by our results will induce structures in the surface and bulk DOS curves that should cause $\alpha(x)$ to be x-dependent. The van Hove singularity associated with the above ETT arises from a BM in the band structure, and the DOS at E_F traverses a mild discontinuity as the Fermi surface undergoes this ETT. The discontinuity is broadened by the disorder inherent in the alloy [11], and moreover is sampled in these experiments as an integral over the DOS. For these reasons, the rate of rigid band shift is modified only slightly through the ETT, in qualitative accord with the results in figure 8.

We now discuss the effect of the observed ETT on the electronic DOS and, as a result, the electron–phonon coupling λ. λ depends linearly on $N(E_F)$ [36], and in turn helps to determine the superconducting transition temperature T_c. T_c should therefore be modified in the vicinity of an ETT [9], although what parameters actually produce the variation in superconducting transition temperature T_c in transition metal alloys has been the subject of considerable debate [28, 37]. For Mo_xRe_{1-x} alloys, T_c increases monotonically as a function x, for $0 \leqslant x \leqslant 0.4$, with no significant anomaly observed near the ETT [24, 28]. This observation argues against a direct connection between the ETT and T_c. The thermopower exhibits a maximum near $x = 0.1$, and this might be related to the ETT.
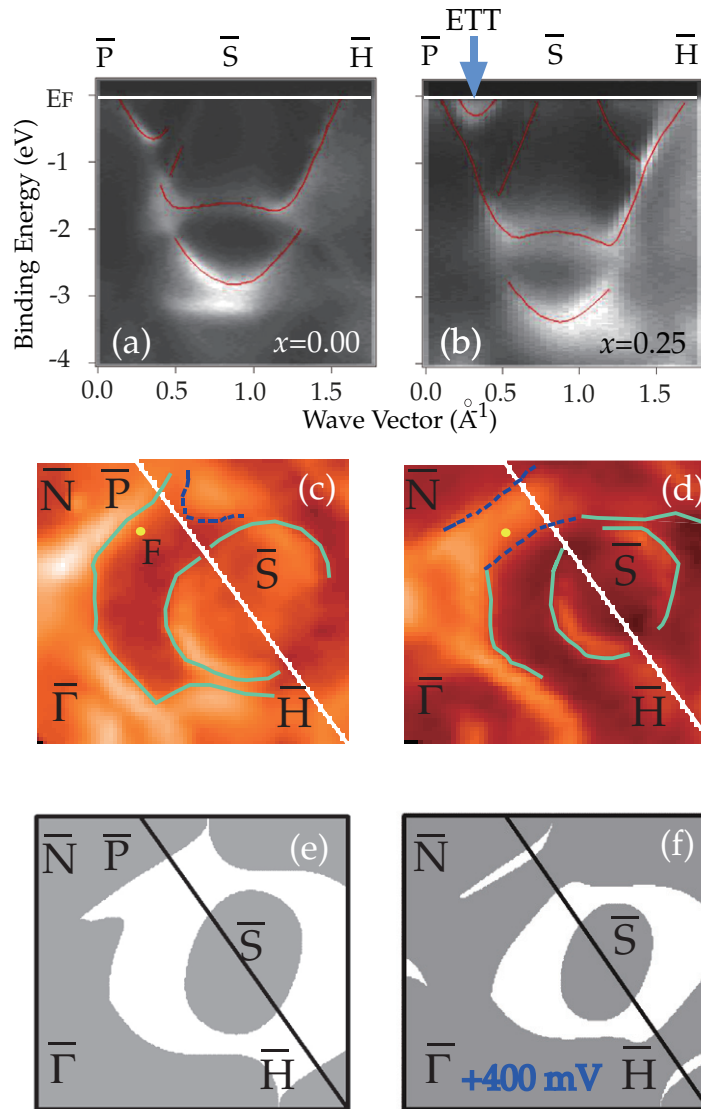
Figure 9. Panels (a) and (b): valence band maps of $Mo_{1-x}Re_x(110)$ for (a) $x = 0.00$ and (b) $x = 0.25$, along the $\overline{P} - \overline{S} - \overline{H}$ direction on the SBZ. The superposed curves indicate the underlying dispersion relations. The extra feature near E_F on the alloy surface (marked with vertical arrow) indicates the movement of a BM through the Fermi level from above. (c), (d) Experimentally determined Fermi surface of $Mo_{1-x}Re_x$ projected on the (110) SBZ for (c) $x = 0.00$ and (d) $x = 0.25$. The yellow F point indicates the starting point of ETT predicted by theoretical calculations. The blue dotted lines are guides for eyes to indicate the extent of the topological transition. (e), (f) Calculated projections of bulk molybdenum band structure onto the (110) SBZ at energies corresponding to electron counts in $Mo_{1-x}Re_x$ for alloy concentrations (e) $x = 0.00$ and (f) $x = 0.25$.

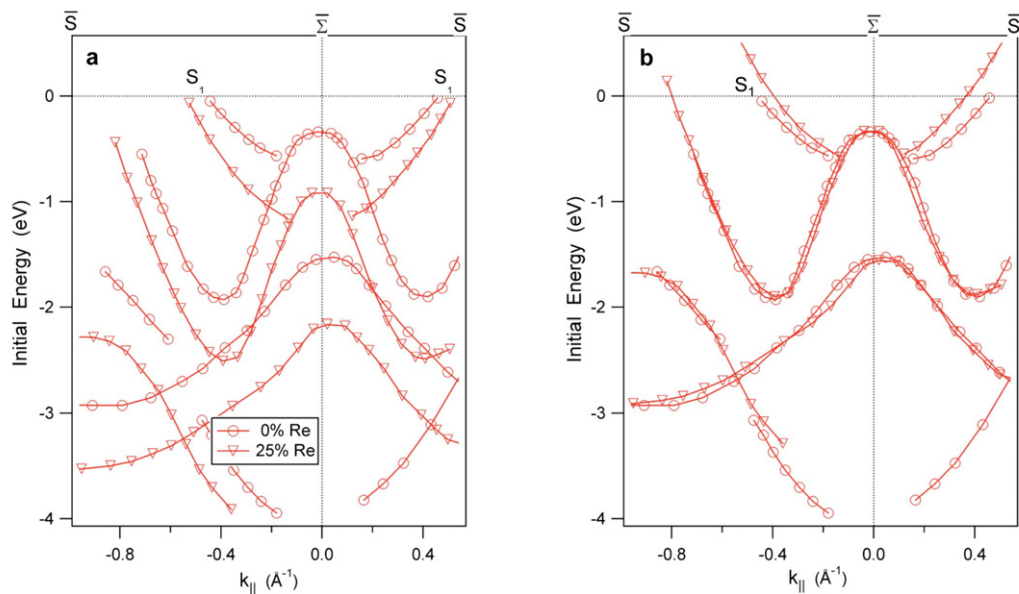**Figure 10.** (a) Bands measured along the $\overline{S} \to \overline{S}$ line in the SBZ for pure Mo(110) and for $Mo_{0.75}Re_{0.25}(110)$. As in figure 7(a), the approximate rigid band behavior is apparent. (b) Bands from panel (a) shifted and stretched accordingly as in figure 7(c). The bands now overlay, with the exception of the highly surface localized band labeled S_1.

4.3. Deviations from rigid band behavior

Slight modification of the RBM accounts for most of our results; there are two notable deviations from this simple behavior. The first involves the highly surface-localized surface state that drives a deep surface phonon anomaly on Mo(110)-(1 × 1)H and the closely related surface W(110)-(1 × 1)H [38–43]. Figure 10(a) presents bands measured along the $\overline{S} \to \overline{S}$ line in the SBZ for pure Mo(110) and for $Mo_{0.75}Re_{0.25}(110)$. As was observed in figure 7(a), the approximately rigid shift of most bands is readily apparent. Upon applying the shift and stretch algorithm from section 4.1 to these data, most of the alloy bands do indeed collapse onto those of the pure molybdenum surface. However, the state labeled S_1 (using the same nomenclature as in previous papers [42, 43]) exhibits a clear deviation from this trend—a lower than predicted shift. Similar deviations are observed for this state along other lines in the SBZ. In group VIB metals, the Fermi level falls near a minimum in the bulk DOS. In this case, the local DOS near the Fermi level in the surface layer is probably higher than in the bulk due to the existence of surface states and resonances. Our results confirm qualitatively the expectation that the modified surface LDOS should substantially alter the rigid band behavior of a surface localized state—a higher LDOS would naturally lead to a slower band shift with alloy composition. Indeed, the surface localization of this state varies along its dispersion. As the band approaches the bulk continuum near the $\overline{\Sigma}$ line, it will gradually lose its surface localization, and the shift and stretch algorithm brings the alloy band into a fairly close alignment with that on the pure surface. Away from the $\overline{\Sigma}$ line, the band lies in the middle of large band gaps and is highly surface localized and, consequently, a pronounced deviation from RB behavior is observed.
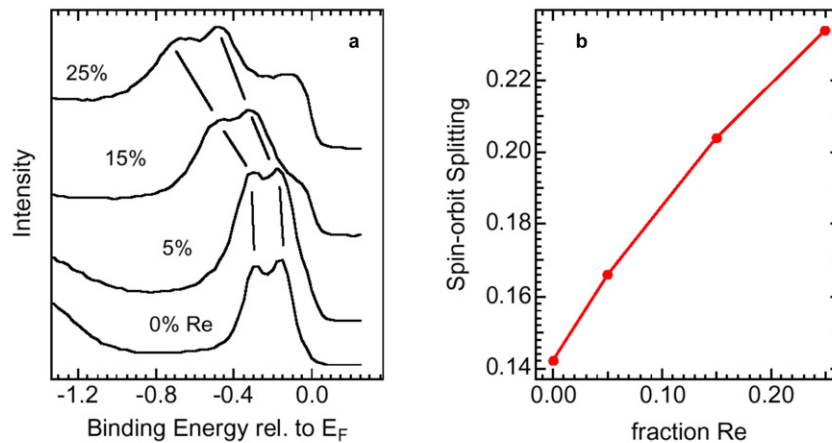
Figure 11. (a) Spin–orbit splitting as a function of Re content. Spectra taken at the bottom of the surface ETT band along $\bar{P}$–$\bar{H}$, showing the maximum splitting. (b) The spin–orbit splitting derived from quantitative curve-fitting of these data as a function of coverage.

The other deviation from rigid band behavior pertains to the surface-related spin–orbit splitting of surface states [44–47]. This splitting is related to the magnitude of the surface potential gradient and also approximately scales with the atomic spin–orbit parameter [48]. It is, for example, four to five times smaller on the 4d metal surface Mo(110) than on the 5d W(110) surface [45]. In this system, it is most clearly evident and most easily studied on the hydrogen-covered surfaces near the ETT along the $\bar{P} \to \bar{H}$ line of the SBZ. Figure 11(a) shows photoemission spectra in this region for the hydrogen-saturated surfaces. The dominant feature near E_F is the S_1 surface state that has been split by the spin–orbit interaction. It is apparent in the spectra that the splitting increases with rhenium concentration. The evolution of the spin–orbit splitting with composition is displayed in figure 11(b). Clearly, introduction of 5d rehenium atoms into a 4d molybdenum host increases the average atomic spin–orbit parameter and, therefore, the surface-related spin–orbit splitting. The change in splitting is two to three times larger than the precision with which equation (1) collapses the alloy bands onto those of pure molybdenum, i.e. this represents a significant deviation from rigid-band behavior. Such data provide a serious challenge to existing surface electronics structure calculations, which rarely include the spin–orbit interaction and which essentially never address alloy surfaces.

5. Summary and conclusions

In summary, using angle-resolved photoemission we have observed approximately rigid shifts of surface and bulk bands for $Mo_{1-x}Re_x(110)$ in the range $x = 0$–0.25. We distinguished two contributions to these shifts, one pertaining to increasing Fermi energy and the other to the increasing overall bandwidth. The Fermi energy shift is inversely related to the bulk DOS near the Fermi level. KKR-CPA calculations accurately predict our experimental results. We also characterized an ETT of the bulk Fermi surface and related this to bulk transport properties. Finally, we discussed two surface-related deviations from the above behavior.

Acknowledgments

References

[1] Zinkle S J and Ghoniem N M 2011 *J. Nucl. Mater.* **417** 2
[2] Mott N F and Jones W 1958 *Theory of the Properties of Metals and Alloys* (Oxford: Oxford University Press)
[3] Raimes S 1962 *J. Phys. Radium* **23** 639
[4] Hüfner S and Wertheim G K 1973 *Phys. Rev.* B **8** 4511
[5] Sellmeyer D J 1978 *Solid State Physics* ed F Seitz and D Turnbull vol 33 (New York: Academic) p 83
[6] Friedel J 1958 *Nuovo Cimento* **7** 287
[7] Cohen M H and Heine V 1958 *Adv. Phys.* **7** 395
[8] Anderson P W 1961 *Phys. Rev.* **124** 41
[9] Crossey-Favre A, Boyen H G and Oelhafen P 1995 *Phys. Rev.* B **52** 16410
[10] Becker C and Hafner J F 1995 *J. Phys.: Condens. Matter* **7** 5843
[11] Skorodumova N V *et al* 1998 *Phys. Rev.* B **57** 14673
[12] Velikodnyi A N *et al* 1986 *JETP Lett.* **43** 773
[13] Yarmoshenko Y M *et al* 1986 *Fiz. Met. Metalloved.* **62** 932
[14] Skorodumova N V *et al* 1994 *JETP Lett.* **60** 565
[15] Kamihara Y *et al* 2008 *J. Am. Chem. Soc.* **130** 3296
[16] Balatsky A V and Parker D 2009 *Physics* **2** 59
[17] Liu T *et al* 2010 *Nature Mater.* **9** 718
[18] He X *et al* 2011 *Phys. Rev.* B **83** 220502
[19] Nandi S *et al* 2010 *Phys. Rev. Lett.* **104** 057006
[20] Wilkinson I *et al* 2001 *Phys. Rev. Lett.* **87** 216401
[21] Vitos L, Abrikosov A and Johansson B 2001 *Phys. Rev. Lett.* **87** 156401
[22] Abrikosov I A, Olovsson W and Johansson B 2001 *Phys. Rev. Lett.* **87** 176403
[23] Hammer L *et al* 1999 *Surf. Sci.* **431** 220
[24] Bruno E *et al* 1994 *Phys. Rep.* **249** 353
[25] Lifshitz I M 1960 *Sov. Phys.—JETP* **11** 1130
[26] Varlamov A A, Egorov V S and Pantsulaya A V 1989 *Adv. Phys.* **39** 469
[27] Blanter Y M *et al* 1994 *Phys. Rep.* **245** 159
[28] Collver M M and Hammond R H 1971 *Phys. Rev. Lett.* **30** 92
[29] Stocks G M, Temmerman W M and Gyorffy B L 1978 *Phys. Rev. Lett.* **41** 339
[30] Stocks G M and Winter H 1982 *Z. Phys.* B **46** 95
[31] Faulkner J S and Stocks G M 1980 *Phys. Rev.* B **21** 3222
[32] Johnson D D *et al* 1986 *Phys. Rev. Lett.* **56** 2088
[33] Johnson D D *et al* 1990 *Phys. Rev.* B **41** 9701

[34] Bruno E and Ginatempo B 1997 *Phys. Rev.* B **55** 12946
[35] Papaconstantopoulos D A 1986 *Handbook of the Band Structure of Elemental Solids* (New York: Plenum)
[36] McMillan W L 1968 *Phys. Rev.* **167** 331
[37] Moruzzi V L *et al* 1983 *Phys. Rev.* B **27** 2049
[38] Hulpke E and Lüdecke J 1993 *Surf. Sci.* **287/288** 837
[39] Hulpke E and Lüdecke J 1992 *Phys. Rev. Lett.* **68** 2846
[40] Kohler B *et al* 1995 *Phys. Rev. Lett.* **74** 1387
[41] Kohler B *et al* 1996 *Z. Phys. Chem.* **197** 193
[42] Rotenberg E and Kevan S D 1998 *Phys. Rev. Lett.* **80** 2905
[43] Rotenberg E, Schäfer J and Kevan S D 2000 *Phys. Rev. Lett.* **84** 2925
[44] LaShell S, McDougall B A and Jensen E 1996 *Phys. Rev. Lett.* **77** 3419
[45] Rotenberg E, Chung J W and Kevan S D 1999 *Phys. Rev. Lett.* **82** 4066
[46] Hochstrasser M *et al* 2002 *Phys. Rev. Lett.* **89** 216802
[47] Nicolay G *et al* 2001 *Phys. Rev.* B **65** 033407
[48] Petersen L and Hedegrad P 2000 *Surf. Sci.* **459** 449